Critical Region for Amyloid Fibril Formation of Mouse Prion Protein: Unusual Amyloidogenic Properties of the Helix 2 Peptide[†]

Kei-ichi Yamaguchi, Tomoharu Matsumoto, and Kazuo Kuwata*

Center for Emerging Infectious Diseases, Gifu University, Yanagido 1-1, Gifu 501-1194, Japan

Received August 18, 2008; Revised Manuscript Received October 29, 2008

ABSTRACT: To gain insight into the structural mechanism of the conformational conversion process of prion, we examined the potential amyloidogenic property of each secondary structural element in a mouse prion protein (mPrP) and discriminated their relative significance for the formation of amyloid fibrils. Although peptides corresponding to α-helix 2 and α-helix 3 (named H2 peptide and H3 peptide, respectively) formed the amyloid-like fibrils, their structures were quite different. H2 fibrils formed the ordered β-sheet with the β-turn conformation, and the resultant fibrils were long and straight. In contrast, H3 fibrils consisted of the β-sheet with the random conformation, and the resultant fibrils were short and flexible. These properties are basically consistent with their hydrophobicity and β-strand propensity profiles. To examine the cross reactivity between peptide fragments and full-length mPrP, we then carried out seeding experiments. While H2 seeds induced the formation of fibrils of full-length mPrP as quickly as full-length mPrP seeds, H3 seeds exhibited a long lag time. This implies that the region of α-helix 2 rather than α-helix 3 in mPrP has great potential for initiating fibril formation. As a whole, the α-helix 2 region would be crucial for the nucleation-dependent replication process of the prion protein.

Transmissible spongiform encephalopathies make up a group of neurodegenerative diseases mainly affecting mammalian species, including humans and cattle. The pathogenesis in these unusual diseases is associated with the conformational rearrangement of a cellular isoform of prion protein (PrP^C)[1] to a scrapie isoform (PrP^{Sc}) in the brain (*1*−*4*). While the PrP^C conformer is monomeric and rich in the α-helical conformation, PrP^{Sc} is characterized by an increased proportion of β-sheet, partial resistance to proteinase K digestion, and occasional formation of amyloid fibrils (*5, 6*). In contrast to high-resolution data for monomeric PrP^C (*7*), the structure of PrP^{Sc} remains unknown.

To understand the molecular pathogenesis of prion diseases, it is essential to elucidate the atomic structure of a PrP^{Sc}. Historically, the segment involving residues ∼90−140 has been known to be important for the PrP^C to PrP^{Sc} conversion (*8*−*10*). Formation of amyloid fibrils has been reported for a number of synthetic peptides derived from the PrP90−145 sequence (*11, 12*), often at nonphysiological pH or in the presence of organic solvents (*13*−*15*). Structurally, the best-characterized of these is PrP106−126, in which the β-sheet core of the amyloid maps to the central part of the peptide (residues 111−123) (*15*). Guided by electron microscopic images of two-dimensional (2D) crystals, Govaerts et al. proposed a structural model for PrP^{Sc} in which residues 89−175 form the left-handed β-helix that associates into trimers (*16*), whereas the entire C-terminal region retains the native α-helical conformation of PrP^C.

Meanwhile, a redacted recombinant PrP of 106 amino acids with two deletions (Δ23−88 and Δ141−176) was shown to retain the ability to support PrP^{Sc} formation in transgenic mice and form β-sheet-rich aggregates in vitro (*8, 17*). This result implies that the core region of PrP^{Sc} involves the C-terminal α-helical regions in PrP^C. Recently, Lu et al. (*18*) performed the H−D exchange analysis for the structure of amyloid fibrils formed by recombinant human PrP90−231 and mapped the H-bonded β-sheet core of PrP amyloid to the C-terminal region (starting at residue ∼169) that in the native structure of a PrP monomer corresponds to α-helix 2, a major part of α-helix 3, and the loop between these two helices. No extensive hydrogen bonding was detected in the N-terminal part of PrP90−231 fibrils, arguing against the stable left-handed β-helix model (*16*). However, it is not yet understood which of helices 2 and 3 are more important and essential for the formation of the H-bonded β-sheet core of PrP amyloid.

In this work, we synthesized a series of peptide fragments corresponding to secondary structural elements throughout the whole mouse PrP (mPrP) and examined the potential amyloidogenic property. We found that only two peptides composed of α-helix 2 or α-helix 3, corresponding to the β-sheet core of PrP90−231 fibrils (*18*), formed amyloid-like fibrils. To gain further insight into the amyloidogenic

[†] This work was supported by the Program for the Promotion of Fundamental Studies in Health Science of the National Institute of Biomedical Innovation and by a grant from Research on Measures for Intractable Diseases (Prion Disease and Slow Virus Infections) of the Ministry of Health, Labour and Welfare of Japan. K.K. and K.Y. were supported in part by Grants-in-Aid for Scientific Research from the Ministry of Education, Culture, Sports, Science and Technology of Japan and grants from the Ministry of Health, Labour and Welfare.

* To whom correspondence should be addressed: Center for Emerging Infectious Diseases, Gifu University, 1-1 Yanagido, Gifu 501-1194, Japan. Fax: +81-58-230-6144. E-mail: kuwata@gifu-u.ac.jp.

[1] Abbreviations: CD, circular dichroism; EM, electron microscope; FTIR, Fourier transform infrared spectroscopy; Gdn-HCl, guanidine hydrochloride; pI, isoelectric point; PrP^C, cellular form of prion protein; PrP^{Sc}, scrapie form of prion protein; ThT, thioflavin T.

10.1021/bi801562w CCC: $40.75
Published on Web 11/16/2008

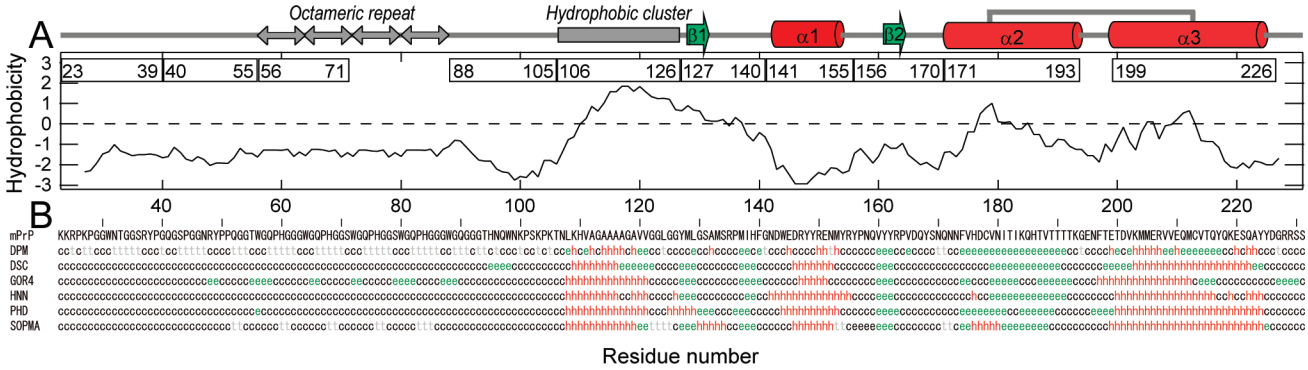

FIGURE 1: Primary structure analyses of mPrP. The secondary structural elements determined on the basis of the NMR structure (PDB entry 1AG2) and octameric repeat and hydrophobic cluster are shown schematically at the top. (A) Predicted hydrophobic profile of mPrP (*50*). The regions of 10 peptides synthesized here are indicated by bars, in which the residue numbers of the peptides are specified. (B) Probabilities of secondary structure predicted by DPM (*51*), DSC (*52*), GOR4 (*53*), HNN (*54*), PHD (*55*), and SOPMA (*56*) algorithms indicated by h (helix), e (sheet), t (turn), and c (coil). These algorithms were executed with ANTHEPROT (*57*).

properties of these peptides, we examined the optimal pH conditions for fibril formation and compared the fibrils produced by α-helix 2 and 3 peptides using circular dichroism (CD), Fourier transform infrared (FTIR), and an electron microscope (EM) in detail. The results showed that the structures of the fibrils made from α-helix 2 and 3 peptides were quite different, and the cross reaction occurred efficiently between α-helix 2 fibrils and full-length mPrP, suggesting the importance of the α-helix 2 region in the formation of fibrils of prion protein.

EXPERIMENTAL PROCEDURES

Peptide Fragments. The peptides for investigation were selected on the basis of their secondary structure (*7*) and the functional region (*19*) of mouse PrP (Figure 1). The sequences of 10 peptides were synthesized here: PrP23−39 (KKRPKPGGWNTGGSRYP), PrP40−55 (GQGSPGGNRYPPQGGT), PrP56−71 (WGQPHGGGWGQPHGGS), PrP88−105 (WGQGGGTHNQWNKPSKPK), PrP106−126 (TNLKHVAGAAAAGAVVGGLGG), PrP127−140 (YMLGSAMSRPMIHF), PrP141−155 (GNDWEDRYYRENMYR), PrP156−170 (YPNQVYYRPVDQYSN), PrP171−193 (QNNFVHDCVNITIKQHTVTTTTK), and PrP199−226 (ETDVKMMERVVEQMCVTQYQKESQAYYD). The mouse PrP106−126 peptide studied here is homologous to residues 107−127 of human PrP. The 10 peptides were synthesized with Fmoc chemistry using a PS-3 peptide synthesizer (Protein Technologies, Tucson, AZ). The cleaved peptides were purified (>95%) by reversed phase HPLC using a COSMOSIL $5C_{18}$-AR-II column (Nacalai Tesque, Kyoto, Japan). Molecular weights of the peptides were determined by matrix-assisted laser desorption ionization time-of-flight (MALDI-TOF) mass spectrometry (Bruker Daltonics, Billerica, MA).

Polymerization Assay. Fibril formation of peptides was performed at 37 °C using a final peptide concentration of 100 μM. The following buffers were used: glycine-HCl (pH 1.9−3.5), acetate-NaOH (pH 4.0−5.5), phosphate-NaOH (pH 6.2−7.5), Tris-HCl (pH 7.8−8.8), and glycine-NaOH (pH 9.2−10.0). The concentration of buffers was 25 mM, and all contained 100 mM NaCl. First, the lyophilized peptides were dissolved in H_2O. Only the lyophilized peptide of PrP199−226, corresponding to α-helix 3 of mPrP, was dissolved in the solution of 50% (v/v) acetonitrile and 5 mM HCl. Stock solutions were then diluted 10-fold in the buffer solutions, and the mixture was incubated at 37 °C. In fibril formation of full-length mPrP23−231, first lyophilized mPrP was dissolved in H_2O and diluted in the buffer solutions containing 150 mM NaCl and 2 M Gdn-HCl to a final mPrP concentration of 10 μM. The mixture was then ultrasonicated at 37 °C.

In seeding experiments, sonicated mPrP fibrils formed at pH 5.5 and 7.5 were added at a final monomer concentration of 0.5 μM to reaction mixtures at pH 5.5 and 7.5, respectively, containing 10 μM mPrP, 150 mM NaCl, and 2 M Gdn-HCl. In the experiments using peptide seeds, sonicated H2 fibrils formed at pH 5.5 and H3 fibrils formed at pH 7.0 were added at a final monomer concentration of 2.5 μM to the reaction mixtures of mPrP at pH 5.5. The solutions were incubated at 37 °C with ultrasonication.

Ultrasonication-Induced Fibril Formation. A water bath-type ultrasonic transmitter with an ELESTEIN 070-GOT temperature controller (Elekon, Chiba, Japan) was used to induce the formation of full-length mPrP fibrils. The volume of the water bath was ∼12 L. The frequency of the instrument was 17−20 kHz, and the power output was set to deliver a maximum of 350 W. Reaction mixtures were ultrasonicated from three directions (i.e., two sides and bottom) for 30 s and then incubated for 9 min without sonication, and the process was repeated during an incubation at 37 °C.

ThT Fluorescence and CD Measurements. Fluorescence measurements were performed using an RF-5300PC spectrofluorophotometer (Shimadzu, Kyoto, Japan). The excitation and emission wavelengths were 445 and 485 nm, respectively, with the reaction mixture containing 10 μM thioflavin T (ThT) (Wako Pure Chemical Industries, Osaka, Japan) and 50 mM sodium phosphate buffer (pH 7.5). From each reaction tube, 10 μL aliquots were subjected to fluorescence spectroscopy. Fluorescence was measured immediately after the mixture was made, averaged for the initial 3 s.

CD spectra were recorded at 25 °C on an AVIV model 215s spectropolarimeter with a step size of 0.2 nm. Far-UV CD spectra of amyloid fibrils and monomers of various pH values were measured using a quartz cell with a light path of 1 mm and a peptide concentration of 0.1 mg/mL. The

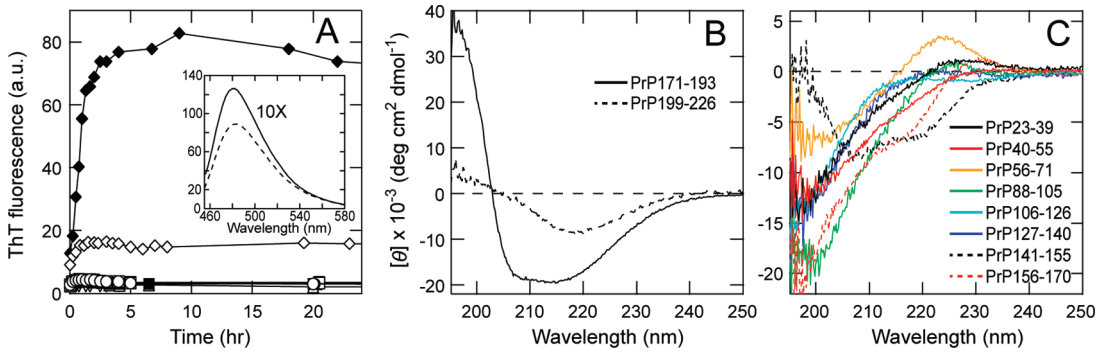

FIGURE 2: Formation of fibrils by 10 peptide fragments of mPrP at pH 5.5. (A) Spontaneous fibril growth at 37 °C monitored by a fluorometric assay with ThT. Reaction mixtures contained 100 μM PrP23−39 (○), PrP40−55 (●), PrP56−71 (□), PrP88−105 (■), PrP106−126 (△), PrP127−140 (▲), PrP141−155 (▽), PrP156−170 (▼), PrP171−193 (◇), or PrP199−226 (◆), 25 mM acetate-NaOH, and 100 mM NaCl. The inset shows the ThT spectra of H2 (PrP171−193) and H3 (PrP199−226) fibrils indicated by solid and dotted lines, respectively. The spectrum of H2 was measured at a 10-fold concentration of fibrils. (B) CD spectra of fibrils formed by H2 (PrP171−193) and H3 (PrP199−226) peptides after incubation for 2 days. (C) CD spectra of peptide fragments after incubation for 7 days. These peptides did not exhibit an increase in ThT fluorescence. The PrP56−71 peptide corresponding to two repeats of octameric repeat exhibited a unique CD spectrum with a peak at 224 nm, as reported in the previous study (*19*).

results are expressed as mean residue ellipticity [θ] (degrees square centimeters per decimole).

FTIR Measurements. ATR-FTIR spectra were recorded with a Bruker Tensor 27 FTIR spectrometer (Bruker Optics, Billerica, MA) equipped with a liquid N_2-cooled mercury cadmium telluride (MCT) detector and a BioATR II unit. The sample solutions were centrifuged (35000*g* at 4 °C for 30 min) to precipitate the fibrils after incubation for 2 days. The precipitated fibrils were loaded onto the surface of a BioATR II prism, and the spectra were recorded at 25 °C with a resolution of 4 cm^{-1} and were averaged for 128 scans. From the spectrum of each sample, a corresponding buffer spectrum was subtracted. The secondary structure contents were estimated by deconvolution analysis of amide I. FTIR spectra were subjected to Fourier self-deconvolution and the second-derivative calculation to estimate the number of peaks and the appropriate peak wavenumbers of the Gauss function. All FTIR spectra were fitted with Gauss functions without restricting the peak wavenumbers. Thus, the most probable frequency was obtained, and the bandwidth for all peak positions was determined. The secondary structure contents were calculated from the area of the fitted Gauss function. The assignments of Gauss functions are summarized in Table 1, and the peaks of side chains were fitted in the 1599−1607 cm^{-1} region. Second derivatives of FTIR spectra were presented after normalizing the total amide I absorptions by the main chain for protein concentrations.

EM Observations. A 2 μL aliquot of the sample solution was placed on a copper grid (400 mesh) covered with carbon film for 1 min, and excess solution was removed by blotting with filter paper. The grid was negatively stained with a 5 μL droplet of 2% uranyl acetate for 1 min. Again, the liquid on the grid was removed by blotting, and the grid was dried. Electron micrographs were taken using a JEM-1010 transmission EM (JEOL, Tokyo, Japan), operating at an 80 kV acceleration with a magnification of 40000×.

RESULTS

Amyloid Fibril Formation of Peptide Fragments of mPrP at pH 5.5. Among the peptides that were examined, PrP199−226 corresponding to the region of α-helix 3 of mPrP (Figure 1), named H3 peptide, showed a significant increase in thioflavin T (ThT) fluorescence (Figure 2A), and PrP171−193 corresponding to α-helix 2 of mPrP, named H2 peptide, showed only a slight increase in ThT fluorescence. However, we clearly observed amyloid-like fibrils of H2 peptide with the EM (Figure 5), and the maximum wavelengths of their ThT fluorescence were both around 480 nm (Figure 2A, inset). Thus, we assumed that the affinity of ThT molecules for H2 fibrils is low, as reported for other amyloid fibril systems (*20, 21*). We then examined the secondary structure of these fibrils using CD at pH 5.5. The CD spectrum of H3 fibrils revealed a β-sheet conformation with a minimum at 218 nm (Figure 2B). However, the CD spectrum of H2 fibrils exhibited a nadir of ~214 nm and a large negative ellipticity, which was significantly distinct from that of H3 fibrils.

Although the PrP106−126 peptide is the most hydrophobic region in mPrP, it did not show an increase in ThT fluorescence even after incubation for 7 days (Figure 2A). The CD spectrum of PrP106−126 showed a random conformation after 7 days (Figure 2C). It is possible that the concentrations of the peptide and salt used in this experiment were lower than those in previous studies (*13*−*15*). The peptides of other regions did not show any increase in ThT fluorescence even after incubation for 7 days (Figure 2A). The CD spectra of these peptides exhibited an almost random conformation with a minimum of ~200 nm (Figure 2C). Among the random peptides, the PrP141−155 peptide, which is relatively short and corresponds to α-helix 1 of mPrP, named the H1 peptide, was suggested to form a partially folded α-helical conformation.

pH Dependence of Amyloid Fibril Formation. To examine the optimum pH value for fibril formation, we initially examined the formation of fibrils of all peptides at pH 2.5 and 8.5. As a result, only H2 and H3 peptides exhibited increased ThT fluorescence, but the intensity of the H2 peptide was quite lower than that of the H3 peptide at both pH values. Since it is difficult to detect fibril formation of the H2 peptide by the ThT fluorescence assay, we used CD spectroscopy to investigate the pH dependence of fibril formation.

First, we examined the pH dependence of fibril formation of the H2 peptide after incubation for 2 days at 37 °C.

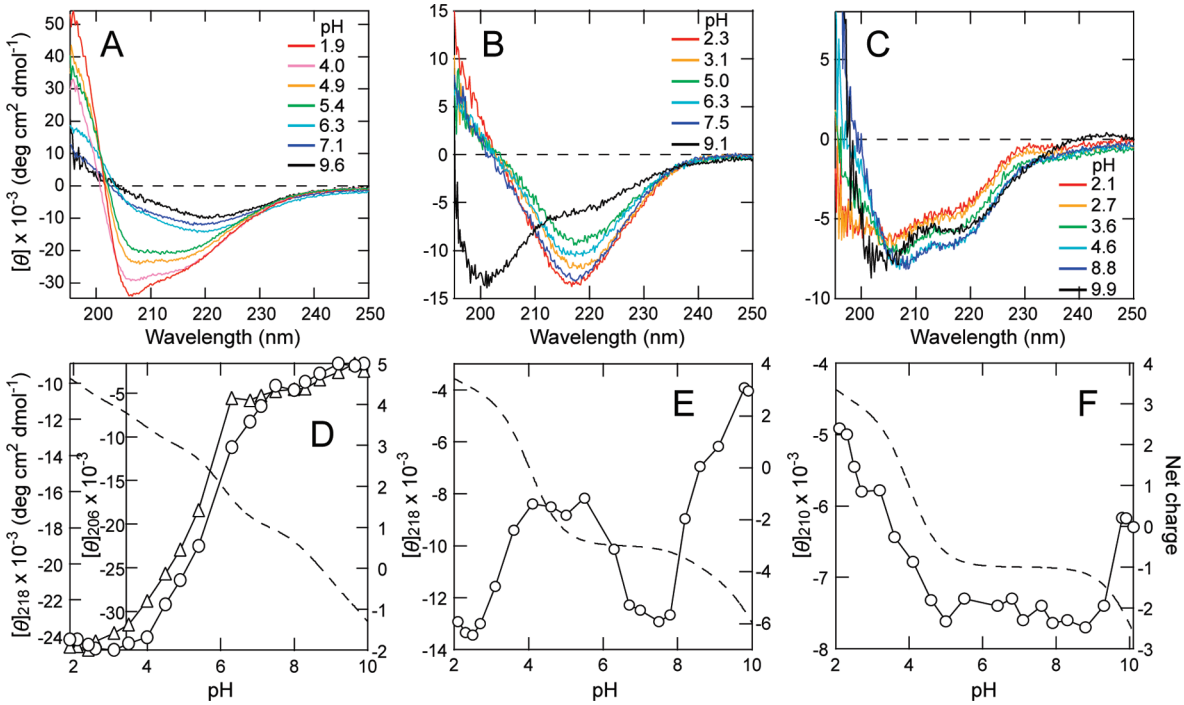

FIGURE 3: pH-dependent conformational change of three peptides corresponding to helical regions of mPrP^C. (A−C) CD spectra of H2 (A), H3 (B), and H1 (C) peptides after incubation for 2 days under various pH conditions. (D−F) Conformational changes of H2 fibrils monitored as ellipticity at 218 (○) and 206 nm (△) (D), H3 fibrils monitored as ellipticity at 218 nm (E), and the H1 monomer monitored as ellipticity at 210 nm (F). In panels D−F, the net charge of peptides is indicated by dashed lines (right ordinate). The pI values of H2, H3, and H1 peptides are 8.6, 4.1, and 4.6, respectively.

Unexpectedly, H2 fibrils showed a unique CD spectrum with a minimum at 206 nm and large negative ellipticity (−34000 deg cm^2 dmol^{-1}) at pH 1.9 (Figure 3A). Although this CD spectrum resembles that of the helical conformation in appearance, its large negative ellipticity would indicate an ordered conformation of amyloid-like fibrils. At basic pH, the CD spectra exhibited a β-sheet conformation with low ellipticity (Figure 3A). The pH dependence of the conformational transition was monitored at 218 and 206 nm, respectively, exhibiting dramatic conformational change around pH 5−6 (Figure 3D). The isoelectric point (pI) of the H2 peptide is pH 8.6. Around pI, the CD intensity gradually decreased, suggesting the formation of aggregate-like fibrils due to the neutralization of electric repulsion between peptides.

The CD spectrum of the H3 peptide showed a typical β-sheet conformation in the pH range of 2−8 (Figure 3B). Although the transition curve of H3 fibrils is significantly distinct from that of H2 (Figure 3D,E), the CD intensity of both H3 and H2 fibrils commonly decreased around each pI value (the pI of the H3 peptide is 4.1), suggesting the formation of aggregates. Although amyloid fibrils often grow to be 1−2 μm long, the turbidity of amyloid fibrils is relatively low (Figure S1 of the Supporting Information), and thus, the CD spectra of fibrils are normally measured (*22, 23*). Actually, all the fibril solutions without H3 aggregates were clear. H3 aggregates at pH ∼5.0 showed the small amount of particles, which could cause a decrease in the magnitude of the CD signal and a slight shift in wavelength due to the light scattering (Figure 3B). At basic pH, the increase in the level of charge repulsion between H3 peptides suppressed the formation of amyloid fibrils.

We also examined the conformational change in the H1 peptide. H1 monomer, which formed a partially folded α-helix at pH 5.5, showed a helix−coil transition depending on pH (Figure 3C). The conformational transition was monitored at 210 nm (Figure 3F) and revealed that H1 monomer formed partially folded α-helix in the pH range of 5−9, though H1 is a short peptide consisting of only 15 amino acids. This result is consistent with the intrinsically high helical propensity of α-helix 1 in mPrP (Figure 1B).

Subsequently, we examined the kinetics of fibril formation of H2 and H3 peptides by CD and ThT fluorescence measurements, respectively. The CD intensity of the H2 peptide increased with time, and unusual H2 fibrils with a minimum at 206 nm and large negative ellipticity were formed at pH 2.5 (Figure 4A). The CD spectra during the fibril formation of the H2 peptide constituted an isodichroic point, implying that the formation of H2 fibrils can be explained by a simple two-state model. We estimated the fraction of the extended fibrils along the time course at various pH values (Figure 4B). The formation of both H2 and H3 aggregates at pH 8.0 and 5.0, respectively, near these pIs was actually fast and reached equilibrium ∼3 h after initiation of the reaction (Figure 4B,C). The fibril formation of H2 and H3 peptides at pH 2.5 was completed after incubation for 10 and ∼22 h, respectively. The fibril formation of the H3 peptide at pH 8.0, however, was fast, and its ThT intensity was higher than at other pH values (Figure 4C), suggesting the further formation of amyloid-like fibrils. The notable increase in ThT fluorescence at this early stage might be caused by the contamination of aggregates (Figure 4C).

Amyloid-like Fibrils Observed with an EM. EM observations revealed that H2 peptide formed many straight amyloid-like fibrils with a diameter of 10−15 nm at pH 2.5 (Figure 5A). A mature H2 fibril was composed of a few protofilaments whose diameter was 3−4 nm (Figure 5G). At pH 5.0,

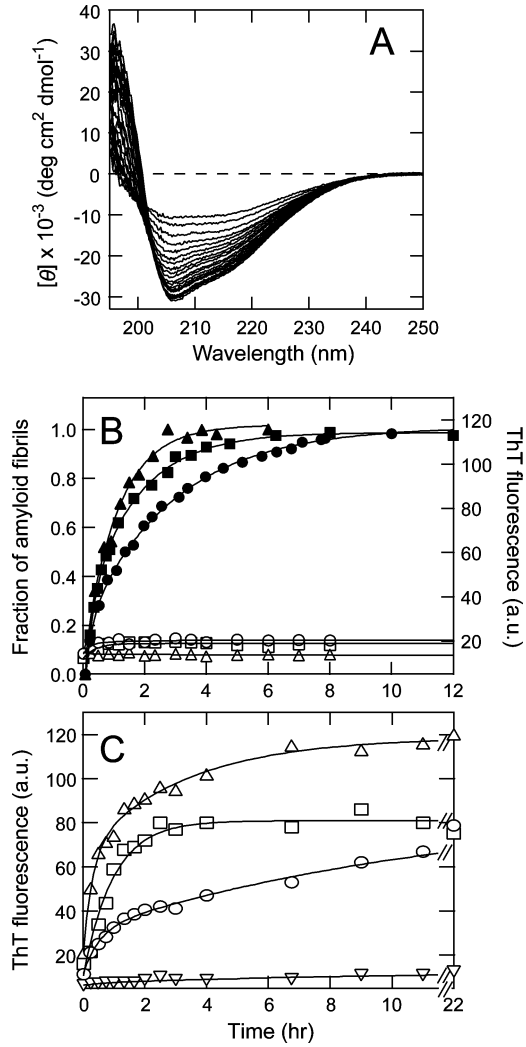

FIGURE 4: Fibril formation of H2 and H3 peptides under various pH conditions. (A) CD spectra of H2 fibrils at pH 2.5. Series of spectra measured after various periods of incubation were overlaid: the stronger the intensity at 206 nm, the longer the incubation time. (B) Time courses of fibril formation of the H2 peptide at pH 2.5 (●), 5.0 (■), and 8.0 (▲) were monitored by CD spectroscopic analysis (left ordinate) and at pH 2.5 (○), 5.0 (□), and 8.0 (△) by ThT fluorescence analysis (right ordinate). (C) Time courses of fibril formation of the H3 peptide at pH 2.5 (○), 5.0 (□), 8.0 (△), and 9.5 (▽) were monitored by ThT fluorescence.

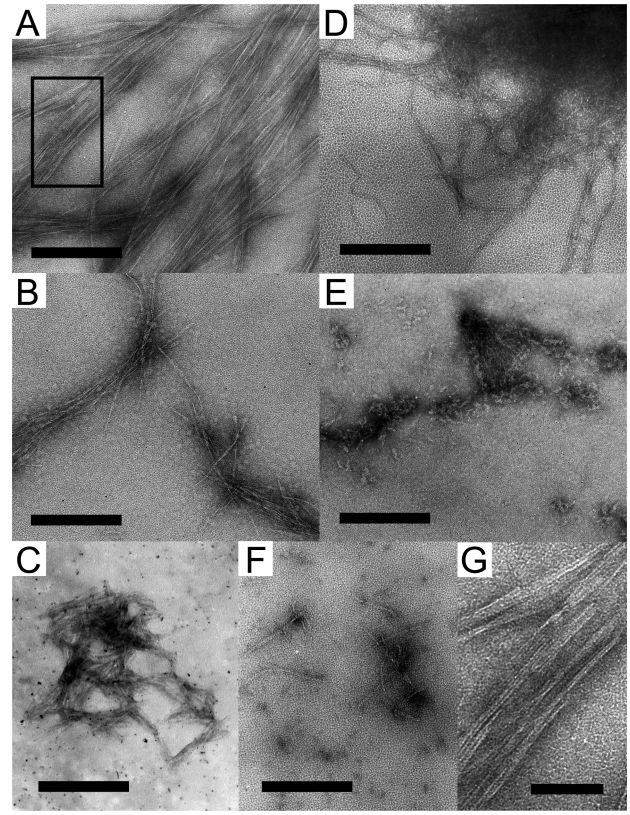

FIGURE 5: EM images of H2 and H3 peptides after incubation for 2 days. (A−C) Amyloid- or aggregate-like fibrils of the H2 peptide were prepared at pH 2.5 (A), 5.0 (B), and 8.0 (C). (D−F) Amyloid-like fibrils or aggregates of the H3 peptide were prepared at pH 2.5 (D), 5.0 (E), and 8.0 (F). Scale bars are 300 nm. (G) Magnified image of H2 fibrils at pH 2.5 taken from panel A. The magnified region is indicated by the square in panel A. The scale bar is 100 nm.

relatively thin and short fibrils were observed (Figure 5B), and at pH 8.0 near its pI, short and aggregate-like fibrils were mainly observed (Figure 5C). In contrast, the H3 peptide formed flexible fibrils with a diameter of 5−10 nm at pH 2.5 far from its pI (Figure 5D), whose morphology differed significantly from that of rigid H2 fibrils. At pH 8.0, relatively thin and short fibrils were observed (Figure 5F); nevertheless, at pH 5.0 near its pI, nonfibrillar aggregates were observed (Figure 5E). Amyloid-like fibrils of H2 were confirmed with the EM, but ThT fluorescence almost never increased (Figure 2A). We employed another criterion for amyloid fibrils, binding with Congo red dye (*24*). When the dye bound to H2 fibrils, the absorbance at ~540 nm was increased at all pH values (data not shown). The presence of H2 fibrils was verified by using Congo red.

Table 1: Secondary Structure Assignments and IR Band Positions for the Amide I Band of Different Forms of H2 and H3 Fibrils

secondary structure assignment	percentage of secondary structure contents[a] pH 2.5 [band position (cm^{-1})]	pH 5.0 [band position (cm^{-1})]	pH 8.0 [band position (cm^{-1})]
H2 fibrils			
intermolecular β-sheet (parallel)	59.7 (1623)	55.3 (1622)	44.4 (1621)
β-sheet	10.0 (1635)	10.4 (1633)	17.0 (1637)
random	9.8 (1646)	11.6 (1645)	17.6 (1651)
turn/loop	20.5 (1663, 76, 90)	22.7 (1666,81, 95)	21.0 (1667, 82, 96)
H3 fibrils			
intermolecular β-sheet (antiparallel[b])	46.8 (1616, 91)	41.9 (1617, 92)	44.8 (1615, 93)
β-sheet	13.7 (1631)	13.7 (1632)	12.9 (1631)
random	20.0 (1642)	26.9 (1645)	21.1 (1643)
turn/loop	19.5 (1659, 74, 88)	17.5 (1661, 75, 88)	21.2 (1660, 77, 87)

[a] The error should be expected in the range of 4−10% in secondary structure analysis as determined by FTIR (*29*). [b] This antiparallel β-sheet structure is attributed to a high-frequency component of the β-sheet. No conclusive assignment for the β-sheet conformation in H3 aggregates at pH 5.0 could be made on the basis of the FTIR data, since two β-sheet components (parallel and antiparallel) might both be present.

Conformation Monitored by FTIR Spectra. Although amyloid-like fibrils of the H2 peptide was confirmed with the EM (Figure 5), its CD spectrum resembled α-helix conformation with a minimum around 206 nm at acidic pH (Figure 3A). We then measured the CD spectra of the H2 monomer in 2,2,2-trifluoroethanol and 10 mM HCl (Figure S2 of the Supporting Information), in which the H2 monomer formed an α-helical conformation. However, the unusual CD spectrum of H2 fibrils was essentially different from that of the α-helical conformation.

To characterize the secondary structure of H2 and H3 fibrils, we measured FTIR spectra in an aqueous solution. As a result, H2 fibrils formed at pH 2.5 and 5.0 exhibited almost identical amide I bands of FTIR spectra (Figure 6A,B). The amide I band (1600−1700 cm^{-1}) is known to be a sensitive probe of secondary structure (*25, 26*). Recently, it was demonstrated that amide I′ peaks in the range of 1611−1630 cm^{-1} are characteristic of the intermolecular β-sheet formed by amyloid fibrils, while bands of native β-sheet clustered between 1630 and 1643 cm^{-1} (*27, 28*). Deconvolution analysis and the second derivative of the FTIR spectrum at pH 2.5 revealed major bands corresponding to an intermolecular β-sheet and a turn conformation with bands at 1623 and 1663 cm^{-1}, respectively (Figure 6A,D). However, the α-helical conformation with a band around 1655 cm^{-1} (*25, 26*) could not be observed. In contrast, the FTIR spectrum of H2 aggregate-like fibrils formed at pH 8.0 near its pI (Figure 6C) was quite distinct from those at acidic pH. Although the FTIR spectrum showed the presence of an intermolecular β-sheet at 1620 cm^{-1} at pH 8.0 (Figure 6C,D), the estimated amount was 44.4% (Table 1), which was smaller than that at pH 2.5 (59.7%), and the presence of a relatively large amount of random conformation with a band of 1651 cm^{-1} at pH 8.0 (Table 1). The differences in intermolecular β-sheet and random contents between H2 fibrils at pH 2.5 and aggregate-like fibrils at pH 8.0 are equal or larger than the error of 4−10% in deconvolution analysis by FTIR (*29*). We considered that the distinction between conformations of H2 fibrils at pH 2.5 and aggregate-like fibrils at pH 8.0 was meaningful. Meanwhile, all H2 fibrils at different pHs showed bands of turn/loop conformations at 1663−1667 cm^{-1}, but these conformations were slightly different (Figure 6D). The second derivative of the spectra showed that H2 fibrils formed at pH 2.5 (solid line) had a band at 1663 cm^{-1}, though H2 fibrils at pH 5.0 (gray line) and pH 8.0 (dotted line) had a band at 1666 and 1667 cm^{-1}, respectively. These bands are affected by types of turn conformations due to the perturbation of the transition dipole coupling (*30, 31*). We considered that the CD spectrum with a minimum at 206 nm seen in ordered H2 fibrils at pH 2.5 was caused by a turn conformation with the band at 1663 cm^{-1} observed only at pH 2.5, and its band could be assigned to a type I or II′ β-turn conformation (see Discussion).

Subsequently, we measured the FTIR spectra of H3 fibrils or aggregates at various pHs, exhibiting an amide I maximum at smaller wavenumbers along with a low-intensity peak associated with an antiparallel intermolecular β-sheet with bands at ∼1616 and ∼1692 cm^{-1}, respectively (Figure 6E−H) (*25*−*27*). However, no conclusive assignment for the β-sheet conformation (parallel or antiparallel) in H3 aggregates at pH 5.0 could be made on the basis of the FTIR data, since two β-sheet components might both be present (*12, 26*).

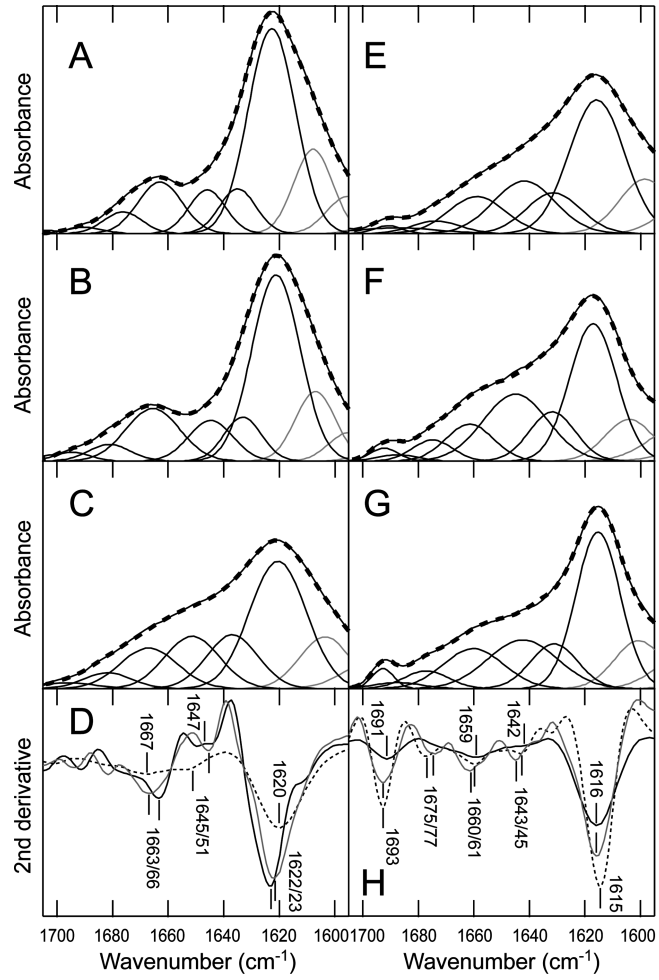

FIGURE 6: FTIR spectra of H2 and H3 fibrils under various pH conditions. (A−C) Absorption spectra of H2 fibrils recorded at pH 2.5 (A), 5.0 (B), and 8.0 (C). (E−G) Absorption spectra of H3 fibrils or aggregates recorded at pH 2.5 (E), 5.0 (F), and 8.0 (G). Deconvolution analysis for the amide I region was performed to determine the secondary structure contents by curve fitting (Table 1). The results of deconvolution analysis of FTIR spectra (solid lines) are shown as dotted lines. Gray peaks represent contributions due to nonsecondary structure. (D and H) Second derivatives of the FTIR spectra of H2 fibrils (D) prepared at pH 2.5 (solid line), pH 5.0 (gray line), and pH 8.0 (dotted line) and H3 fibrils (H) prepared at pH 2.5 (solid line), pH 5.0 (gray line), and pH 8.0 (dotted line). Several β-sheet components are evident at 1615−1623 cm^{-1} and around 1692 cm^{-1}, in addition to random conformations at 1642−1651 cm^{-1} and turn/loop conformations in the range of 1659−1696 cm^{-1}.

For parallel β-sheets, only the low-frequency band around 1611−1630 cm^{-1} is expected (*12, 32*), and usually upshifted by a few wavenumbers (*25*). We suggest, therefore, that the intermolecular β-sheet structure in H2 fibrils with a single band around 1622 cm^{-1} could be predominantly parallel rather than antiparallel (Figure 6D).

Although both H3 fibrils formed at pH 2.5 and 8.0 had bands of intermolecular β-sheet conformations at ∼1616 cm^{-1} and random conformations at ∼1643 cm^{-1} (Figure 6H), their secondary structure contents did not differ much from those of H3 aggregates formed at pH 5.0 (Table 1). Significant differences in secondary structure contents and band positions could not be observed between fibrils at pH 2.5 and 8.0 in this study (Table 1). Those H3 fibrils seemed to be more flexible than the H2 fibrils formed at pH 2.5,

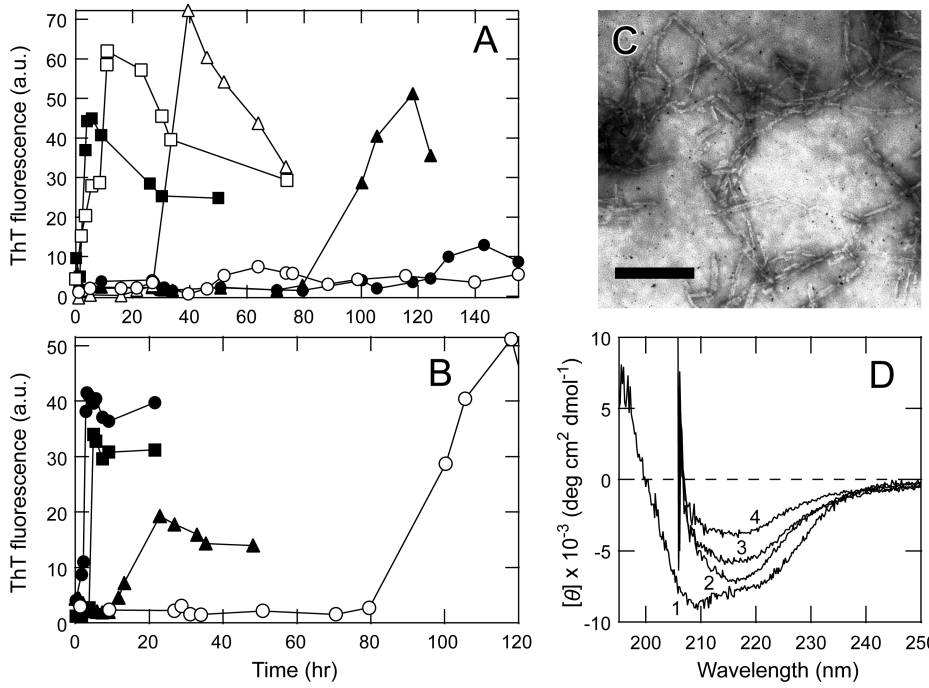

FIGURE 7: Cross reactions of amyloid fibril formation between peptide fragments and full-length mPrP at 37 °C. (A) Spontaneous fibril formation of mPrP without ultrasonication at pH 5.5 (●) and 7.5 (○). Ultrasonication-induced fibril formation of mPrP without seeds at pH 5.5 (▲) and 7.5 (△) and with seeds at pH 5.5 (■) and 7.5 (□). Reaction mixtures contained 10 μM mPrP, 150 mM NaCl, and 2 M Gdn-HCl. mPrP seeds were added at a final monomer concentration of 0.5 μM. (B) Fibril formation of mPrP with ultrasonication at pH 5.5 without seeds (○) taken from panel A, with mPrP seeds (●), with H2 seeds (■), and with H3 seeds (▲). H2 and H3 seeds were added at a final monomer concentration of 2.5 μM. (C) EM image of ultrasonication-induced mPrP fibrils at pH 5.5 with mPrP seeds after incubation for 1 day. The scale bar is 300 nm. (D) CD spectra of mPrP in the native state at pH 5.5 (1) and mPrP fibrils formed by seeding of mPrP fibrils (2), H2 fibrils (3), and H3 fibrils (4).

since the intermolecular β-sheet content of H3 fibrils was much lower than that of H2 fibrils, and the random content of H3 fibrils was higher than that of H2 fibrils (Table 1). These results were consistent with the flexible H3 fibrils at pH 2.5 and 8.0 observed with the EM (Figure 5).

Cross Reactions between Peptide Fragments and Full-Length mPrP. First, we examined the fibril formation of full-length mPrP23−231 using ultrasonication, which is known to induce the formation of amyloid fibrils made by many kinds of proteins, including PrP (*33, 34*). Ultrasonication is one form of agitation triggering the formation of amyloid fibrils. Although mPrP does not form amyloid fibrils for at least several days without ultrasonication at pH 5.5 and 7.5 (Figure 7A), ThT fluorescence increased markedly after a lag time of 70−80 h at pH 5.5 upon sonication of the mPrP solution. At pH 7.5, ThT fluorescence increased more rapidly after a lag time of 20−30 h with sonication, since the pI of mPrP is pH 9.6. We then examined the effects of seeding on the fibril formation of full-length mPrP with ultrasonication. The addition of seeds composed of mPrP fibrils induced the formation of fibrils without a lag time at pH 5.5 and 7.5 (Figure 7A). Many fragmented fibrils were observed with the EM (Figure 7C), because we sonicated the mPrP solution throughout the extension reaction. Full-length mPrP formed thick fibrils with a diameter of 15−20 nm, which was larger than those of H2 and H3 fibrils, and the twist was not clear in mPrP fibrils. mPrP and H3 fibrils seemed to be flexible rather than H2 fibrils (Figures 5A,D and 7C), suggesting that random contents in mPrP and H3 fibrils were larger than that in H2 fibrils.

Subsequently, we examined the cross reactivity between peptide fragments and full-length mPrP at pH 5.5. Upon addition of seeds composed of H2 fibrils, ThT fluorescence increased markedly after a lag time of 2−3 h (Figure 7B), which was much shorter than that of H3 seeds which exhibited a long lag time of 9−14 h. This result indicates that H2 fibrils work more efficiently as seeds in the extension reaction of mPrP fibrils. We then investigated the secondary structure of these fibrils using CD spectroscopy. The native state of mPrP showed the CD spectrum of an α-helical conformation at pH 5.5 (Figure 7D). Both mPrP fibrils formed by seeding of mPrP fibrils and H2 fibrils showed the CD spectra of a β-sheet conformation with large ellipticity, suggesting the formation of amyloid-like fibrils, though the decrease in CD intensity by seeding of H3 fibrils suggested the formation of fibrils contaminated with non-fibrillar aggregates. These results imply that the region of α-helix 2 rather than α-helix 3 in mPrP is more important for initiating fibril formation.

DISCUSSION

Prion's pathogenic conversion reaction is generally considered to be composed of two stages. The first stage may be the unfolding of PrP^C, possibly catalyzed by factor X (*35*). The second stage is a kind of folding process derived by the generic mechanism from the active intermediate state (PrP*) (*36*) or unfolded state (PrP^U) to PrP^{Sc}. The latter is a nucleation-dependent process and somewhat similar to the replication occurring at the extending edge of amyloid fibrils. Although we do not know whether any chaperone factor is actually involved in the latter reaction, such a catalyzing factor may not be obligatory for the nucleation-dependent replication process. Alternatively, the distribution of intrinsic

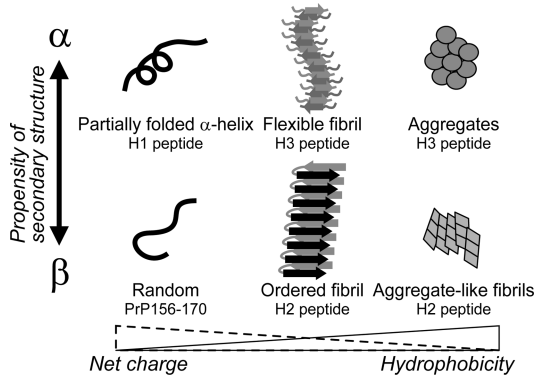

FIGURE 8: Amyloidogenic properties of peptide fragments of mPrP. The hydrophobicity (solid line) and net charge (dashed line) of peptides increase and decrease, respectively, and the balance between hydrophobic and electrostatic interactions is crucial for the formation of amyloid fibrils. The regions of H2 and H3 peptides are fairly hydrophobic among mPrP. The H2 peptide has a high propensity for β-strand intrinsically and formed ordered amyloid-like fibrils with a β-turn conformation. In contrast, the H3 peptide has a high propensity for α-helix, which could suppress the formation of ordered fibrils. Around the pI of the peptides, neutralization of electric repulsion between peptides promotes the formation of aggregates. Far from the pI, repulsion between peptides becomes a barrier for forming fibrils. The H1 peptide, which is hydrophilic and has a propensity for α-helix, formed a partially folded α-helix by itself. PrP156−170, which is hydrophilic and has a propensity for β-strand (Figure 1), formed a random conformation (Figure 2C).

amyloidogenic properties among mPrP sequences is considered to be the central problem in the latter process.

Critical Region for Amyloid Fibril Formation of mPrP. We investigated the fibril formation of a series of peptide fragments corresponding to the secondary structural elements of mPrP. Only H2 and H3 peptides, which were fairly hydrophobic regions in mPrP (Figure 1A), formed amyloid-like fibrils or aggregates. Historically, although the segment involving residues ~90−140 has been known to be important for the PrP^C to PrP^{Sc} conversion (*8*−*16*), recently, Lu et al. revealed that the β-sheet core of PrP amyloid fibrils consisted of the C-terminal region of PrP (starting at residue ~169) (*18*). The amyloidogenic peptides shown in this study were consistent with the region of the β-sheet core of PrP fibrils (*18*). However, the conformations of H2 and H3 fibrils were significantly different. Studies with various mutants of acylphosphatase have demonstrated that hydrophobicity and β-sheet propensity of key regions, as well as the net charge of the protein, are critical factors for aggregation (*37, 38*). Surprisingly, the H2 peptide was predicted to have a high propensity of β-strand among mPrP (Figure 1B), though the helix 2 region formed an α-helix conformation in $mPrP^C$. The high propensity of β-strand and hydrophobicity of the H2 peptide would promote the formation of β-sheet-rich amyloid fibrils (Figure 8). In contrast, although the H3 peptide is hydrophobic, this region is predicted to form α-helix (Figure 1B), so it might be difficult to form β-sheet-rich amyloid fibrils with the H3 peptide rather than with the H2 peptide (Figure 8). Thus, the amyloidogenic property would be basically consistent with their hydrophobicity and β-strand propensity profiles. Meanwhile, the H1 peptide is short, with 15 amino acids, but its monomer formed a partially folded α-helix conformation by itself (Figure 3C). It is considered that the region of α-helix 1 would form an α-helix conformation in $mPrP^C$ spontaneously, which is predicted to be hydrophilic with a propensity for α-helix (Figures 1 and 8). These properties suggest that it may be difficult to form a stable β-sheet core by α-helix 1 in mPrP fibrils.

Extension of mPrP fibrils with mPrP seeds is rapid without a lag time (Figure 7A). On the other hand, heterogeneous reactions between mPrP and peptide fragments exhibited a lag time (Figure 7B). The fibril conformation is probably different between fibrils, and the heterogeneous association of monomers with the end of the seeds would be thermodynamically unfavorable. Extension of mPrP fibrils with H2 seeds is relatively rapid, but seeding of H3 fibrils exhibited a long lag time. These results suggested that H2 fibrils have internal structures similar to mPrP fibrils, which enables seeding of mPrP fibrils. Moreover, the intensities of the ThT fluorescence and CD spectrum of mPrP fibrils seeded by H2 fibrils are higher than those seeded by H3 fibrils. Taken together, it is conceivable that the region of α-helix 2 rather than α-helix 3 in mPrP has a great potential for initiating the fibril formation, which could propagate β-sheet conformation by itself to the rest of the molecule.

Unexpected β-Turn Conformation in Ordered Amyloid Fibrils. Although H2 fibrils exhibited a unique CD spectrum with a minimum at 206 nm at acidic pH (Figure 3A), FTIR measurements revealed that H2 fibrils consisted of an intermolecular β-sheet and a turn conformation, but not α-helix (Figure 6A). The CD spectra of model cyclic peptides, forming β-turn conformations of type I or II′, showed a minimum around 205 nm (*39*−*41*). It is considered that the CD spectrum of H2 fibrils with a minimum at 206 nm would be a combination of β-sheet and type I or II′ β-turn conformations. All FTIR spectra of H2 fibrils at different pHs exhibited bands of turn/loop conformations at 1663−1667 cm^{-1}, but these conformations were slightly different (Figure 6D). Thus, we assigned a band at 1663 cm^{-1} observed only at pH 2.5 to a type I or II′ β-turn conformation, which would be distinct from turn/loop conformations with bands at 1666 and 1667 cm^{-1}.

These CD spectra with a minimum at 206 nm are rarely seen in the monomer state of the globular protein except for α-helix or random conformations but are occasionally seen in amyloid fibrils that form β-sheet and turn conformations (*42*−*44*). In general, naturally abundant β-strands are fewer than 10 residues long (*45*). The 23-residue H2 peptide could form a β-strand−turn−β-strand conformation in amyloid fibrils. This geometry was seen in some kinds of amyloid fibrils (*43, 46, 47*), suggesting that it was a common structural motif of amyloid fibrils.

pH Dependence of Fibril Formation. To gain further insight, first we considered the effects of the net charge on the conformational change of the H1 peptide. The H1 monomer formed a partially folded α-helix in the pH range of 5−9 (Figure 3F). In the native state, the salt bridges are formed between the side chains of Asp or Glu and Arg residues in α-helix 1 (*48*). It is considered that protonation of the side chains of Asp or Glu residues below pH 5 and deprotonation of Tyr residues beyond pH 9 could destabilize the partially folded α-helix conformation of the H1 peptide (Figure 3F). Then, we considered the effects of the net charge on fibril formation. Paz et al. showed with a series of amyloidogenic peptides that a net charge of ±1 was one of

the requisites for determining amyloidogenicity (*49*), and a neutral or higher effective charge on the molecules prevents fibril formation. Under optimal pH conditions for the formation of H2 fibrils, the net charge was ~4 (Figure 3D). Aggregate-like fibrils formed at pH ~6, at which the net charge was 2. On the other hand, the H3 peptide formed aggregates at pH 4−6, a point at which the net charge was between −3 and 3 (Figure 3E). Amyloid-like fibrils of the H3 peptide formed at pH 2−3 and 7−8, and the net charge was between ±3. At basic pH, repulsion between peptides became a barrier for formation of fibrils. Thus, the formation of amyloid fibrils is very sensitive to the net charge of peptides. These results are basically consistent with those of Paz et al. (*49*), since the number of hydrophilic residues of the peptides and the reaction conditions affect fibril formation. Both H2 and H3 peptides are fairly hydrophobic among mPrPs, and the net charge of peptides decreases around these pIs, in which aggregates formed (Figure 8). In contrast, ordered amyloid-like fibrils were formed far from these pIs by taking advantage of moderate repulsion, implying that the balance between hydrophobic and electrostatic interactions is crucial for the formation of ordered fibrils.

In conclusion, only H2 and H3 peptides, which are fairly hydrophobic regions in mPrP, formed amyloid-like fibrils or aggregates. In particular, the H2 peptide has a high propensity for β-strand formation among mPrPs, which formed ordered amyloid-like fibrils. H2 fibrils rather than H3 fibrils induced the formation of full-length mPrP fibrils efficiently, implying that α-helix 2 constitutes both the initiation and β-sheet core region in mPrP fibrils. These results strongly suggest that, although the rigid native fold of PrP under physical conditions prevents the formation of amyloid fibrils, the C-terminal region, including α-helix 2, has an intrinsic amyloidogenic preference. Thus, once the native structure is destabilized under conditions where the region of helix 2 is accessible by the seeds or as yet unknown additional factors which trigger generic folding, then prion would adopt the new conformation instead of PrP^C.

ACKNOWLEDGMENT

Electron microscopy was performed with the assistance of the Equipment Center for Common Research at the Graduate School of Medicine, Gifu University.

SUPPORTING INFORMATION AVAILABLE

Dynode voltages of peptides at the CD measurements in Figure 3 (Figure S1) and alcohol-induced conformational transition of the H2 monomer at 25 °C (Figure S2). This material is available free of charge via the Internet at http://pubs.acs.org.

REFERENCES

1. Prusiner, S. B. (1998) Prions. *Proc. Natl. Acad. Sci. U.S.A. 95*, 13363–13388.
2. Collinge, J. (2001) Prion diseases of humans and animals: Their causes and molecular basis. *Annu. Rev. Neurosci. 24*, 519–550.
3. Aguzzi, A., and Polymenidou, M. (2004) Mammalian prion biology: One century of evolving concepts. *Cell 116*, 313–327.
4. Weissmann, C. (2004) The state of the prion. *Nat. Rev. Microbiol. 2*, 861–871.
5. Legname, G., Baskakov, I. V., Nguyen, H.-O. B., Riesner, D., Cohen, F. E., DeArmond, S. J., and Prusiner, S. B. (2004) Synthetic mammalian prions. *Science 305*, 673–676.
6. Bocharova, O. V., Breydo, L., Parfenov, A. S., Salnikov, V. V., and Baskakov, I. V. (2005) *In vitro* conversion of full-length mammalian prion protein produces amyloid form with physical properties of PrPSc. *J. Mol. Biol. 346*, 645–659.
7. Riek, R., Hornemann, S., Wider, G., Billeter, M., Glockshuber, R., and Wüthrich, K. (1996) NMR structure of the mouse prion protein domain PrP(121−231). *Nature 382*, 180–182.
8. Muramoto, T., Scott, M., Cohen, F. E., and Prusiner, S. B. (1996) Recombinant scrapie-like prion protein of 106 amino acids is soluble. *Proc. Natl. Acad. Sci. U.S.A. 93*, 15457–15462.
9. Gasset, M., Baldwin, M. A., Lloyd, D. H., Gabriel, J.-M., Holtzman, D. M., Cohen, F., Fletterick, R., and Prusiner, S. B. (1992) Predicted α-helical regions of the prion protein when synthesized as peptides form amyloid. *Proc. Natl. Acad. Sci. U.S.A. 89*, 10940–10944.
10. Tagliavini, F., Prelli, F., Verga, L., Giaccone, G., Sarma, R., Gorevic, P., Chetti, B., Passerini, F., Ghibaudi, E., Forloni, G., Salmona, M., Bugiani, O., and Frangione, B. (1993) Synthetic peptides homologous to prion protein residues 106−147 form amyloid-like fibrils in vitro. *Proc. Natl. Acad. Sci. U.S.A. 90*, 9678–9682.
11. Jones, E. M., and Surewicz, W. K. (2005) Fibril conformation as the basis of species- and strain-dependent seeding specificity of mammalian prion amyloids. *Cell 121*, 63–72.
12. Natalello, A., Prokorov, V. V., Tagliavini, F., Morbin, M., Forloni, G., Beeg, M., Manzoni, C., Colombo, L., Gobbi, M., Salmona, M., and Doglia, S. M. (2008) Conformational plasticity of the Gerstmann-Sträussler-Scheinker disease peptide as indicated by its multiple aggregation pathways. *J. Mol. Biol. 381*, 1349–1361.
13. Salmona, M., Malesani, P., De Gioia, L., Gorla, S., Bruschi, M., Molinari, A., Della Vedova, F., Pedrotti, B., Marrari, M. A., Awan, T., Bugiani, O., Forloni, G., and Tagliavini, F. (1999) Molecular determinants of the physicochemical properties of a critical prion protein region comprising residues 106−126. *Biochem. J. 342*, 207–214.
14. Nguyen, J. T., Inouye, H., Baldwin, M. A., Fletterick, R. J., Cohen, F. E., Prusiner, S. B., and Kirschner, D. A. (1995) X-ray diffraction of scrapie prion rods and PrP peptides. *J. Mol. Biol. 252*, 412–422.
15. Kuwata, K., Matumoto, T., Cheng, H., Nagayama, K., James, T. L., and Roder, H. (2003) NMR-detected hydrogen exchange and molecular dynamics simulations provide structural insight into fibril formation of prion protein fragment 106−126. *Proc. Natl. Acad. Sci. U.S.A. 100*, 14790–14795.
16. Govaerts, C., Wille, H., Prusiner, S. B., and Cohen, F. E. (2004) Evidence for assembly of prions with left-handed β-helices into trimers. *Proc. Natl. Acad. Sci. U.S.A. 101*, 8342–8347.
17. Baskakov, I. V., Aagaard, C., Mehlhorn, I., Wille, H., Groth, D., Baldwin, M. A., Prusiner, S. B., and Cohen, F. E. (2000) Self-assembly of recombinant prion protein of 106 residues. *Biochemistry 39*, 2792–2804.
18. Lu, X., Wintrode, P. L., and Surewicz, W. K. (2007) β-Sheet core of human prion protein amyloid fibrils as determined by hydrogen/deuterium exchange. *Proc. Natl. Acad. Sci. U.S.A. 104*, 1510–1515.
19. Viles, J. H., Cohen, F. E., Prusiner, S. B., Goodin, D. B., Wright, P. E., and Dyson, H. J. (1999) Copper binding to the prion protein: Structural implications of four identical cooperative binding sites. *Proc. Natl. Acad. Sci. U.S.A. 96*, 2042–2047.
20. Khurana, R., Coleman, C., Ionescu-Zanetti, C., Carter, S. A., Krishna, V., Grover, R. K., Roy, R., and Singh, S. (2005) Mechanism of thioflavin T binding to amyloid fibrils. *J. Struct. Biol. 151*, 229–238.
21. Meehan, S., Knowles, T. P. J., Baldwin, A. J., Smith, J. F., Squires, A. M., Clements, P., Treweek, T. M., Ecroyd, H., Tartaglia, G. G., Vendruscolo, M., MacPhee, C. E., Dobson, C. M., and Carver, J. A. (2007) Characterization of amyloid fibril formation by small heat-shock chaperone proteins human αA-, αB- and R120G αB-crystallins. *J. Mol. Biol. 372*, 470–484.
22. Yamaguchi, K., Naiki, H., and Goto, Y. (2006) Mechanism by which the amyloid-like fibrils of a β_2-microglobulin fragment are induced by fluorine-substituted alcohols. *J. Mol. Biol. 363*, 279–288.
23. Fezoui, Y., and Teplow, D. B. (2002) Kinetic studies of amyloid β-protein fibril assembly. *J. Biol. Chem. 277*, 36948–36954.
24. Plakoutsi, G., Bemporad, F., Calamai, M., Taddei, N., Dobson, C. M., and Chiti, F. (2005) Evidence for a mechanism of amyloid

formation involving molecular reorganisation within native-like precursor aggregates. *J. Mol. Biol. 351*, 910–922.
25. Seshadri, S., Khurana, R., and Fink, A. L. (1999) Fourier transform infrared spectroscopy in analysis of protein deposits. *Methods Enzymol. 309*, 559–576.
26. Barth, A., and Zscherp, C. (2002) What vibrations tell us about proteins. *Q. Rev. Biophys. 35*, 369–430.
27. Zandomeneghi, G., Krebs, M. R. H., Mccammon, M. G., and Fändrich, M. (2004) FTIR reveals structural differences between native β-sheet proteins and amyloid fibrils. *Protein Sci. 13*, 3314–3321.
28. Watzlawik, J., Skora, L., Frense, D., Griesinger, C., Zweckstetter, M., Schulz-Schaeffer, W. J., and Kramer, M. L. (2006) Prion protein helix1 promotes aggregation but is not converted into β-sheet. *J. Biol. Chem. 281*, 30242–30250.
29. Goormaghtigh, E., Cabiaux, V., and Ruysschaert, J.-M. (1994) Determination of soluble and membrane protein structure by Fourier transform infrared spectroscopy. III. Secondary structures. *Subcell. Biochem. 23*, 405–450.
30. Bandekar, J., and Krimm, S. (1979) Vibrational analysis of peptides, polypeptides, and proteins: Characteristic amide bands of β-turns. *Proc. Natl. Acad. Sci. U.S.A. 76*, 774–777.
31. Bandekar, J. (1992) Amide modes and protein conformation. *Biochim. Biophys. Acta 1120*, 123–143.
32. Perálvarez-Marín, A., Barth, A., and Gräslund, A. (2008) Time-resolved infrared spectroscopy of pH-induced aggregation of the Alzheimer Aβ_{1-28} peptide. *J. Mol. Biol. 379*, 589–596.
33. Atarashi, R., Moore, R. A., Sim, V. L., Hughson, A. G., Dorward, D. W., Onwubiko, H. A., Priola, S. A., and Caughey, B. (2007) Ultrasensitive detection of scrapie prion protein using seeded conversion of recombinant prion protein. *Nat. Methods 4*, 645–650.
34. Ohhashi, Y., Kihara, M., Naiki, H., and Goto, Y. (2005) Ultrasonication-induced amyloid fibril formation of β_2-microglobulin. *J. Biol. Chem. 280*, 32843–32848.
35. Telling, G. C., Scott, M., Mastrianni, J., Gabizon, R., Torchia, M., Cohen, F. E., DeArmond, S. J., and Prusiner, S. B. (1995) Prion propagation in mice expressing human and chimeric PrP transgenes implicates the interaction of cellular PrP with another protein. *Cell 83*, 79–90.
36. Kuwata, K., Li, H., Yamada, H., Legname, G., Prusiner, S. B., Akasaka, K., and James, T. L. (2002) Locally disordered conformer of the hamster prion protein: A crucial intermediate to PrPSc? *Biochemistry 41*, 12277–12283.
37. Chiti, F., Taddei, N., Baroni, F., Capanni, C., Stefani, M., Ramponi, G., and Dobson, C. M. (2002) Kinetic partitioning of protein folding and aggregation. *Nat. Struct. Biol. 9*, 137–143.
38. Chiti, F., Stefani, M., Taddei, N., Ramponi, G., and Dobson, C. M. (2003) Rationalization of the effects of mutations on peptide and protein aggregation rates. *Nature 424*, 805–808.
39. Hollósi, M., Kövér, K. E., Holly, S., Radics, L., and Fasman, G. D. (1987) β-Turns in bridged proline-containing cyclic peptide models. *Biopolymers 26*, 1555–1572.
40. Gierasch, L. M., Deber, C. M., Madison, V., Niu, C. H., and Blout, E. R. (1981) Conformations of (X-$_L$-Pro-Y)$_2$ cyclic hexapeptides. Preferred β-turn conformers and implications for β-turns in proteins. *Biochemistry 20*, 4730–4738.
41. Rose, G. D., Gierasch, L. M., and Smith, J. A. (1985) Turns in peptides and proteins. *Adv. Protein Chem. 37*, 1–109.
42. Yamaguchi, K., Takahashi, S., Kawai, T., Naiki, H., and Goto, Y. (2005) Seeding-dependent propagation and maturation of amyloid fibril conformation. *J. Mol. Biol. 352*, 952–960.
43. Iwata, K., Fujiwara, T., Matsuki, Y., Akutsu, H., Takahashi, S., Naiki, H., and Goto, Y. (2006) 3D structure of amyloid protofilaments of β_2-microblobulin fragments probed by solid-state NMR. *Proc. Natl. Acad. Sci. U.S.A. 103*, 18119–18124.
44. Saiki, M., Honda, S., Kawasaki, K., Zhou, D., Kaito, A., Konakahara, T., and Morii, H. (2005) Higher-order molecular packing in amyloid-like fibrils constructed with linear arrangements of hydrophobic and hydrogen-bonding side-chains. *J. Mol. Biol. 348*, 983–998.
45. Sternberg, M. J. E., and Thornton, J. M. (1977) On the conformation of proteins: An analysis of β-pleated sheets. *J. Mol. Biol. 110*, 285–296.
46. Tycko, R. (2006) Molecular structure of amyloid fibrils: Insights from solid-state NMR. *Q. Rev. Biophys. 39*, 1–55.
47. Wasmer, C., Lange, A., Van Melckebeke, H., Siemer, A. B., Riek, R., and Meier, B. H. (2008) Amyloid fibrils of the HET-s(218−289) prion form a β solenoid with a triangular hydrophobic core. *Science 319*, 1523–1526.
48. Morrissey, M. P., and Shakhnovich, E. I. (1999) Evidence for the role of PrP^C helix 1 in the hydrophilic seeding of prion aggregates. *Proc. Natl. Acad. Sci. U.S.A. 96*, 11293–11298.
49. López De La Paz, M., Goldie, K., Zurdo, J., Lacroix, E., Dobson, C. M., Hoenger, A., and Serrano, L. (2002) De novo designed peptide-based amyloid fibrils. *Proc. Natl. Acad. Sci. U.S.A. 99*, 16052–16057.
50. Kyte, J., and Doolittle, R. F. (1982) A simple method for displaying the hydropathic character of a protein. *J. Mol. Biol. 157*, 105–132.
51. Deléage, G., and Roux, B. (1987) An algorithm for protein secondary structure prediction based on class prediction. *Protein Eng. 1*, 289–294.
52. King, R. D., and Sternberg, M. J. E. (1996) Identification and application of the concepts important for accurate and reliable protein secondary structure prediction. *Protein Sci. 5*, 2298–2310.
53. Garnier, J., Gibrat, J. F., and Robson, B. (1996) GOR method for predicting protein secondary structure from amino acid sequence. *Methods Enzymol. 266*, 540–553.
54. Guermeur, Y. (1997) Combinaison de classifieurs statistiques, Application a la prediction de structure secondaire des proteines. Ph.D. Thesis, Université Paris 6, France.
55. Rost, B., and Sander, C. (1993) Prediction of protein secondary structure at better than 70% accuracy. *J. Mol. Biol. 232*, 584–599.
56. Geourjon, C., and Deléage, G. (1995) SOPMA: Significant improvements in protein secondary structure prediction by consensus prediction from multiple alignments. *Comput. Appl. Biosci. 11*, 681–684.
57. Deléage, G., Combet, C., Blanchet, C., and Geourjon, C. (2001) ANTHEPROT: An integrated protein sequence analysis software with client/server capabilities. *Comput. Biol. Med. 31*, 259–267.

BI801562W